

## Article

# Seismic Response Analyses of a Large-Span Powerhouse Cavern Considering Rock–Structure Interaction

Yumei Lv<sup>1</sup>, Lichuan Wang<sup>2,3,\*</sup>, Yu Chen<sup>4</sup>, Lun Gong<sup>3</sup> and Shibo Li<sup>5</sup>

<sup>1</sup> Department of Railway Engineering, Shijiazhuang Institute of Railway Technology, Shijiazhuang 050041, China; doudou1841\_0@163.com

<sup>2</sup> China Railway 18 Bureau Group Co., Ltd., Tianjin 300222, China

<sup>3</sup> School of Civil Engineering, Southwest Jiaotong University, Chengdu 610031, China; gonglun33@126.com

<sup>4</sup> China Railway Design Corporation, Tianjin 300308, China; sdschenyu@126.com

<sup>5</sup> Guoneng Shuohuang Railway Development Co., Ltd., Beijing 100080, China; lishibo82@163.com

\* Correspondence: wlc773747@163.com

**Abstract:** Underground structures in earthquake-prone zones should be designed to withstand both static overburden pressures and earthquake shocks. This paper presents a case study on a large-span powerhouse cavern. With seismic data selected from past earthquake records, lab and in situ tests of the cavern's geological and geomechanical conditions were performed to analyze the static and dynamic stability of the cavern through the continuum modeling approach. Performance analyses via both 2D and 3D modeling were carried out under seismic conditions and for selected design ground motions. The dynamic response of the surrounding rock mass and of the reinforcement system was detected. The results obtained will facilitate future stability analyses of large underground caverns constructed in the past on the basis of seismic design analyses and input data from post-earthquake records that were recently made available on the site.

**Keywords:** powerhouse cavern; FEM equivalent continuum modeling; 2D and 3D dynamic analyses; rock mass; Hoek–Brown model; rock–structure interaction



**Citation:** Lv, Y.; Wang, L.; Chen, Y.; Gong, L.; Li, S. Seismic Response Analyses of a Large-Span Powerhouse Cavern Considering Rock–Structure Interaction. *Appl. Sci.* **2022**, *12*, 6649. <https://doi.org/10.3390/app12136649>

Academic Editor: Dario De Domenico

Received: 10 May 2022

Accepted: 27 June 2022

Published: 30 June 2022

**Publisher's Note:** MDPI stays neutral with regard to jurisdictional claims in published maps and institutional affiliations.



**Copyright:** © 2022 by the authors. Licensee MDPI, Basel, Switzerland. This article is an open access article distributed under the terms and conditions of the Creative Commons Attribution (CC BY) license (<https://creativecommons.org/licenses/by/4.0/>).

## 1. Introduction

Stability analysis of large-span underground caverns at the design stage, during construction, and in service is a very challenging work in underground excavation engineering. Historically, underground facilities have experienced a lower rate of seismically induced damage than surface structures. Nevertheless, some underground structures have experienced significant damage in recent large earthquakes, including the 1976 Tangshan, China earthquake; the 1995 Kobe, Japan earthquake; the 1999 Chi-Chi, Taiwan, China earthquake; the 1999 Kocaeli, Turkey earthquake; the 2004 Niigata, Japan earthquake; and the 2008 Wenchuan, China earthquake, and some more recent earthquakes such as the 2016 Kumamoto, Japan earthquake, and the 2016 Norcia, Italy earthquake [1–8]. In particular, the Daikai subway station collapse, the first collapse of an urban underground structure due to earthquake forces rather than ground instability [1], significantly changed the public belief that underground structures had the ability to sustain earthquakes with little damage. Underground structures, varying widely in shape and size, refer to many lifeline facilities such as pipelines for water, sewage, gas, electricity and telecommunication, subways, roads, storage tanks, parking lots, and common utility tunnels. While earthquakes, as some of the most devastating natural disasters, may lead to damage to crucial underground structures such as those associated with the electrical transmission and distribution, water supply, transportation and communication, and even disaster prevention and rescue systems, resulting in catastrophic disasters.

According to the available data, the seismic damage of underground structures includes three main categories, i.e., damage from ground shaking, damage from fault displacement, and damage from ground failure. The major factors for shaking-caused damage

are: (1) the shape, dimensions, and depth of the structure; (2) the properties of the surrounding soil or rock; (3) the material properties of the structure; and (4) the severity of the ground shaking [9–11]. Nowadays, with the increasing number of underground structures with large cross-sections compared with less information on their seismic behaviors, it is imperative to carry out relevant seismic analysis. Analytical methods are usually limited to simple computational models and ideal seismic inputs [12]. Modern performance-based design methods require detailed seismic response analysis of the rock–structure system to investigate the seismic performance and fragility of underground structures under earthquake events [13–17]. More efficient numerical methods should be developed for practical complex models, especially three-dimensional models capable of accurately simulating the seismic response due to the additional seismic loadings, which induce stress redistribution and three-dimensional deformation.

In this paper, following geological and geomechanical investigations with laboratory and in situ testing, a complete sophisticated numerical model is constructed for the seismic response analyses of a large-span powerhouse cavern considering rock–structure interaction. The seismic input is selected from the past earthquake records, corresponding to the seismic characteristics of the site. Although the site is not located in a high-magnitude seismogenic zone, the dynamic modeling studies are of significance to underline the approach adopted.

## 2. Project Background

The hydroelectric plant of concern has been built to replace the old one to enhance the hydraulic production capacity. Compared with the plants previously built, the new plant, with the flowing water controlled daily, will double the production of electricity and quintuple the capacity, and can provide a total power of 27 MW and an average annual electricity production of 200 GWh. This will help to reduce the huge electricity deficit of the region (now about 60% of its needs) and cut the import of a significant amount of fuel.

The overall perspective view of the scheme is shown in Figure 1, and it mainly consists of the following components: the intake, which is located on the river at 1046 m asl; the dam, from which a minimum flow of 1000 l/s can be derived; the 14 km long diversion tunnel, with a gradient of about 1/1000 to supply daily the basin (560,000 m<sup>3</sup>); the 4 km long pressure tunnel, which leads the water to the upper surge tank and finally to the 1.3 km long penstock with an average diameter of 3.2 m; the powerhouse cavern, where two turbines (design flow 17 m<sup>3</sup>/s, speed 750 rpm) are coupled to an 85 MVA generator; and the 1.6 km long outlet tunnel, which returns water into the reservoir (420,000 m<sup>3</sup> capacity) after the downstream surge tank. One of the two above-mentioned turbines is also equipped with a pump, which has a design flow of 13.5 m<sup>3</sup>/s so that the water could be raised from the lower reservoir to the upper lake during the night time.

The central powerhouse cavern is one of the most imposing components of the scheme. It has significantly large dimensions, with a maximum height of 49 m, a length of 50 m, and a span of about 23 m. It is also noteworthy that the design concepts adopted in this large cavern are not traditional; that is, the large cavern has been excavated and stabilized without the use of a cast-in-place concrete arch for roof support. Great attention has been paid to the design of the cavern.

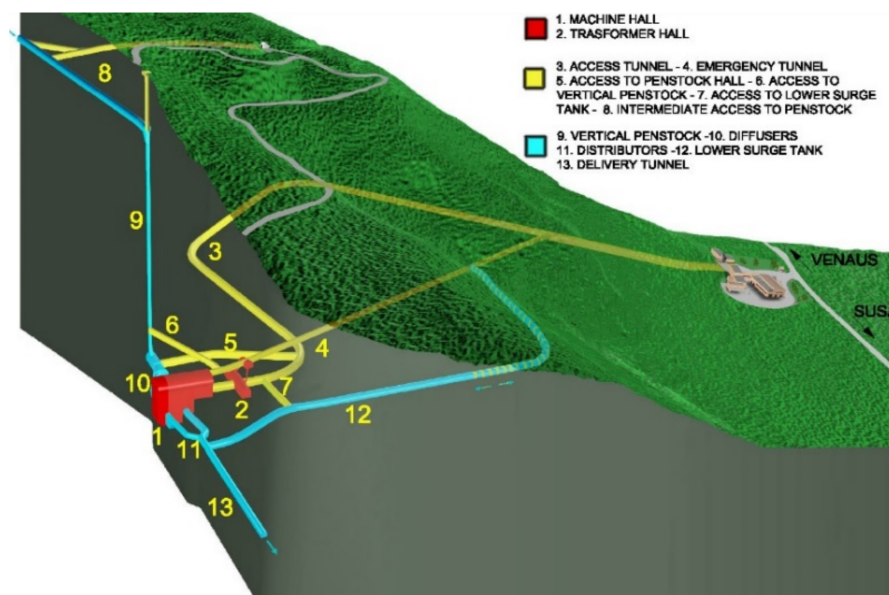


Figure 1. Illustration of the hydroelectric scheme of concern.

### 3. Rock Mass Properties

The cavern has been excavated in a schistose calcschist complex at a depth of 250 m below the ground surface, in a zone where the rock mass is nearly impervious (Figure 2). The structure is more or less foliated and laminated depending on the content of phyllosilicates and graphite, which contributes to the rock mass fissility along the planes of schistosity.

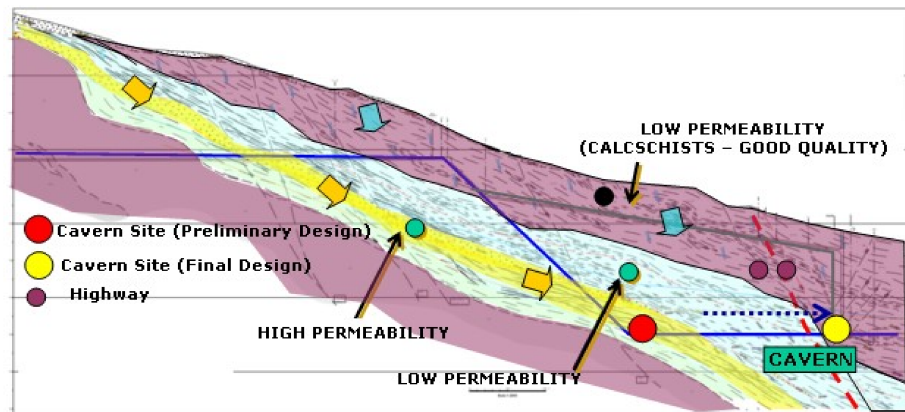


Figure 2. Schematic illustration of the hydro-geological model.

According to research on systematic discontinuity, the rock mass conditions in the cavern can be divided into two zones: Zone 1, chainage 0–25 m, good rock mass quality with RMR 70–75; and Zone 2, chainage 25–50 m, fair rock mass quality with RMR = 56–64. Moreover, the joints and the faults detected are few and most are narrow and closed, without any water flow.

To obtain the physical and mechanical characteristics of the rock mass, a series of surveys were carried out, including laboratory tests on rock cores, in situ rock properties testing, and in situ stress measurements. The main results obtained from the uniaxial compression tests are summarized in Table 1, which also indicates the unit weight, sonic velocity, and Brazilian tensile strength.

**Table 1.** Rock mass parameters calibrated from the triaxial tests.

Deformation Modulus (GPa)		Poisson's Ratio	Intact Rock Compressive Strength (MPa)	Hoek–Brown Model			
Undisturbed	Disturbed			Undisturbed		Disturbed	
				<i>m</i>	<i>s</i>	<i>m</i>	<i>s</i>
22	14	0.25	72.3	1.18	0.012	0.28	0.002

The corresponding parameters of the Hoek–Brown model [18] were calibrated from the triaxial tests, as shown in Table 1.

The deformability of the site was determined by plate load and flat-jack tests near the cavern’s south wall; the plate load tests resulted in a deformational modulus  $E_d$  for the undisturbed rock mass in the range of 20 to 30 GPa, during loading for stress level between 4 and 12 MPa. From the flat-jack tests, which are representative of disturbed rock mass conditions, the corresponding modulus  $E_d$  is in the range of 14 to 20 GPa.

The in situ state of stress in the rock mass surrounding the cavern was determined by hydro-fracturing tests performed in a vertical bore drilled to reach the location of the cavern [19,20]. It could be inferred that the higher principal stresses are approximately normal to the schistosity planes. The state of stress in the horizontal plane is shown to be nearly isotropic with the horizontal stresses being 6.1 MPa, and the vertical stress equal to 10.6 MPa is shown to be slightly greater than the geostatic stress. Accordingly, the stress ratio could be obtained as  $K = 0.57$ . The in situ stress is summarized in Table 2.

**Table 2.** The obtained in situ stress state (unit: MPa).

$\sigma_x$	$\sigma_y$	$\sigma_z$	$\tau_{yz}$	$\tau_{xz}$	$\tau_{xy}$	$\sigma_1$	$\sigma_2$	$\sigma_3$
6.11	6.05	10.58	1.38	−1.87	−1.23	11.8	6.4	4.8

#### 4. Numerical Modeling

In earthquake-prone regions, additional effects occurring around the opening due to earthquake loads should be considered in the design. In seismic design and seismic performance evaluation of buildings, dynamic analyses, also known as response history analyses, are becoming a common practice due to the rapidly increasing computational power and the evolution of engineering software. The goal of seismic design for underground structures is to develop a facility that can withstand a given level of seismic motion with damage not exceeding a predefined resistance level. To evaluate the effects of the seismic motion at a particular site, objective and quantitative descriptions of seismic ground motions are required.

##### 4.1. Selection of the Seismic Input

Selection of input ground motions is a crucial step in the dynamic analysis, because the outcome of the analyses is markedly affected by this choice, thus an accurate estimation of the seismic performance should be carried out based on the seismic hazard at the site where the structures are located. Generally, accelerograms can be defined using different methods as: (1) selecting and scaling real accelerogram (seismic input recorded in real earthquakes), (2) generating artificial records that are compatible with a design response spectrum, and (3) generating synthetic records based on a seismic source model. For the seismic design of some important underground structures such as tunnels and nuclear power plants located in seismically active areas, the real accelerograms, which are recorded in past earthquakes, are still very predominant.

The selected accelerograms, according to EUROCODE 8, need to be representative of the seismicity of the site and be compatible with its seismological and geotechnical characteristics. Several criteria have to be taken into account in the selection of accelerograms for the site of interest.

A suite of not fewer than 3 appropriate ground motions shall be used in the analysis. If at least 7 accelerograms are adopted, average values of response quantities can be used for analysis; on the other hand, if the number of accelerograms is less than 7, the most unfavorable value of the response quantity should be used.

The average response spectrum should be compatible with the target spectrum. In the range of periods of 0.15 s–0.20 s (and 0.2 T<sub>1</sub>–2 T<sub>1</sub>) for horizontal components and the range of 0.15 s–1 s for vertical components, where T<sub>1</sub> is the fundamental period of the structure in the direction where the accelerogram will be applied, no value of the mean 5% damping elastic spectrum, calculated from all time histories, should be less than 90% of the corresponding value of the 5% damping elastic response spectrum [21].

The site where the accelerogram station is installed must be classified as stiff soil or rock so that the local amplification effect can be neglected.

The selected accelerograms must be in accordance with the seismological parameters, that is, magnitude and distance pairs, which are obtained by the deaggregation process.

Seismic hazard analyses should first be performed to determine the seismic parameters, so as to select appropriate real accelerograms. The seismic hazard of the site is characterized by two parameters: the horizontal peak ground acceleration (PGA) and expected macroseismic intensity. The probabilistic seismic hazard maps, generally in terms of these two parameters, can be constructed for areas of different seismogenic regions, showing contours of ground parameter values, to estimate the rate of potential earthquakes across a region and quantify likely ground-shaking levels at a site.

The studied cavern is located in a zone characterized by the horizontal PGA in the 0.10 to 0.15 g range and by the site intensity of VI, with a 10% probability of exceedance in 50 years. The seismic properties can be roughly characterized by design response spectra, which depend on the seismic hazard level as well as geological characteristics of the site. EUROCODE 8 describes the spectral shape distinguishing between horizontal and vertical components of accelerograms. For the horizontal components, the elastic spectral shape is expressed by:

$$0 \leq T \leq T_B : Se(T) = \alpha_g \cdot S \cdot \eta \cdot F_0 \cdot \left[ \frac{T}{T_B} + \frac{1}{\eta \cdot F_0} \left( 1 - \frac{T}{T_B} \right) \right] \tag{1}$$

$$T_B \leq T \leq T_C : Se(T) = \alpha_g \cdot S \cdot \eta \cdot F_0 \tag{2}$$

$$T_C \leq T \leq T_D : Se(T) = \alpha_g \cdot S \cdot \eta \cdot F_0 \cdot \left[ \frac{T_C}{T} \right] \tag{3}$$

$$T_D \leq T \leq 4s : Se(T) = \alpha_g \cdot S \cdot \eta \cdot F_0 \cdot \left[ \frac{T_C T_D}{T^2} \right] \tag{4}$$

where *T* is the vibration period; *a<sub>g</sub>* is the design ground acceleration on type A site class; *S* is the soil factor; *T<sub>B</sub>* and *T<sub>C</sub>* are the limiting periods of the spectrum’s plateau; *T<sub>D</sub>* is the lowest period of the constant spectral portion; and *η* is the damping correction factor, and it is equal to one for 5% viscous damping.

For the studied cavern, the parameters of the design spectrum are shown in Table 3, according to the EUROCODE 8.

**Table 3.** Parameters of design spectrum of the studied cavern for horizontal components.

<i>F<sub>0</sub></i>	<i>a<sub>g</sub></i> (g)	<i>T<sub>B</sub></i> (s)	<i>T<sub>C</sub></i> (s)	<i>T<sub>D</sub></i> (s)	<i>S</i>	<i>η</i>
2.462	0.134	0.088073	0.264218	2.137759	1	1

Based on the adequate knowledge of the seismic hazard of the site, identification of a dominant scenario should be also defined through a process called deaggregation [22] (Reiter, 1991), which aims at estimating the most likely earthquake ground motion records. The primary purpose of deaggregation of the seismic hazard, which in terms of *M* (magni-

tude) and R (distance) displays their contributions to the annual exceedance, is to assist in the determination of earthquake events (M and R) that are physically reasonable and most likely to cause the exceedance, and the determined earthquake events are usually referred to as scenario earthquake events. With the deaggregation process carried out, for the maximum PGA with a 10 percent of exceedance probability in 50 years, a scenario for the site with the magnitude–distance pair of M = 5.3 and R = 19 km was determined.

Selection of Seismic Inputs

Based on the above-mentioned criteria, seven groups of accelerograms in three directions (vertical, N–S, E–W) were selected from the database of the national seismic service for the seismic design of the studied cavern, and the seismological characteristics of the selected accelerograms are summarized in Table 4. Figure 3 shows the comparison between the scaled average response spectra, calculated from the seven groups of accelerograms in the E–W direction, and the target response spectra of horizontal accelerograms, developed by EUROCODE 8 for the cavern site. It can be inferred that the average response spectra are compatible with the target horizontal spectrum, and no value of the mean spectrum is less than 90% of the target spectrum in the period range of 0.15–2 s. The calculated average response spectra in the N–S direction and vertical direction also agree very well with the recommendations of EUROCODE 8.

Table 4. Seismological characteristics of the selected accelerograms.

Code	Acc.	Name	Distance	Date	Mb	ML	MS	MW
410Y	A1	Golbasi (Turkey)	29	5 May 1986	5.7		5.90	
428X	A2	Aetolia (Greece)	23	18 May 1988	5.4	5.3	5.00	
594X	A3	Apennines	11	26 September 1997	5.7	5.8	5.90	5.7
765Y	A4	Apennines	11	12 October 1997	5.2	5.1	5.20	5.3
854X	A5	Apennines	21	3 April 1998	5.1	5.2	4.80	5.1
858X	A6	Apennines	36	3 April 1998	5.1	5.2	4.80	5.1
1314Y	A7	Athens (Greece)	23	7 September 1999	5.8		5.60	5.9

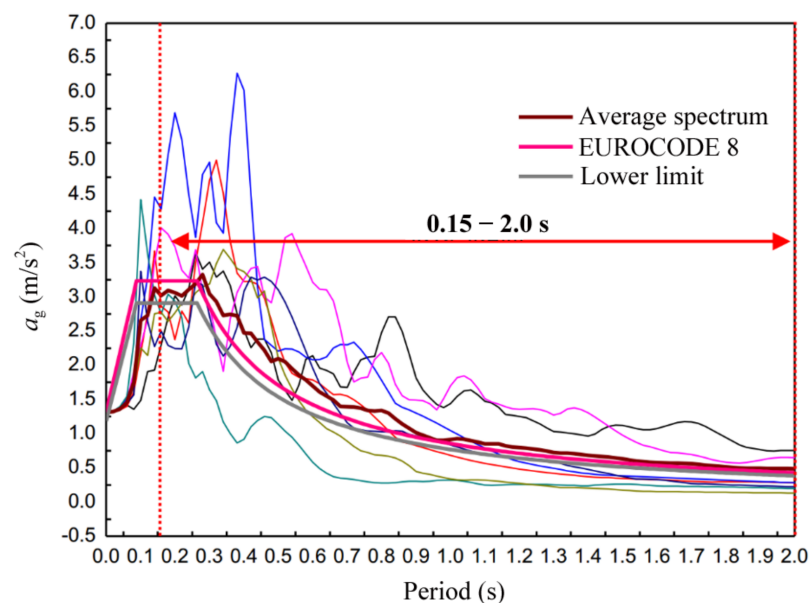
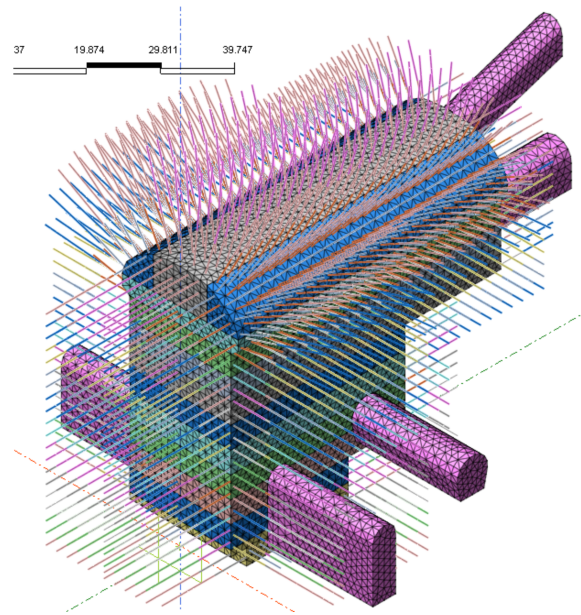


Figure 3. Response spectrum of the selected accelerograms and reference response spectrum.

#### 4.2. 2D and 3D Finite Element Modeling

Continuum modeling by the finite element method (FEM) with the Midas/GTS code was performed in two- and three-dimensional conditions. The implicit modified Newton–Raphson method in Midas/GTS code is used to capture the nonlinearity of the complex rock–structure system, in which the tangent stiffness is updated in each time step based on deformation [23]. Because of the dimension and complex geometry of this cavern, the three-dimensional analysis of the cavern was also performed with the purpose of validating the two-dimensional analysis, as shown in Figure 4. The seismic response of the underground cavern was studied by applying the above-selected accelerograms (Table 4).



**Figure 4.** Reinforcement system adopted in the three-dimensional numerical model.

Zero-thickness Goodman interface elements are used to represent the rock–structure interaction behavior [24]. High normal and shear stiffnesses were set to avoid the occurrence of overlapping. To ensure that the most appropriate methods of modeling are used, the following assumptions/conditions are introduced:

No sliding at the rock–structure interface is assumed to occur (no-slip condition);

Kinematic rock–structure interaction effects are ignored;

Appropriate mechanical damping, representative of the materials under study, has to be determined. The critical damping ratio is taken to be equal to 5%, according to the average value of natural material damping in dynamic conditions;

For accurate representation of wave transmission through a numerical model, the spatial element size,  $l$ , must be smaller than approximately one-tenth to one-eighth of the wavelength associated with the highest frequency component of the input wave, which can be expressed by [25,26]:

$$1 \leq \frac{\lambda}{8 \sim 10} \quad (5)$$

Appropriate boundary conditions should be applied in the analysis: in order to simulate an infinitely extended medium, viscous boundaries are introduced at both the vertical sides of the model;

The recorded accelerograms are assumed directly applied at the bottom of the numerical model.

In both the 2D and 3D models, the bottom boundary was fixed in the vertical direction and viscous boundaries were applied along the lateral boundaries. The filtered input motions were applied at the bottom boundary of the models.

### 5. Results and Discussion

#### 5.1. 2D Analyses

The dynamic analyses using the 2D model were performed first, with the purpose to obtain the seismic response of the cavern when subjected separately to seismic inputs in the E–W, vertical, and both directions. With only the accelerogram A1 adopted, the deformed shapes of the cavern cross-section obtained are shown in Figure 5.

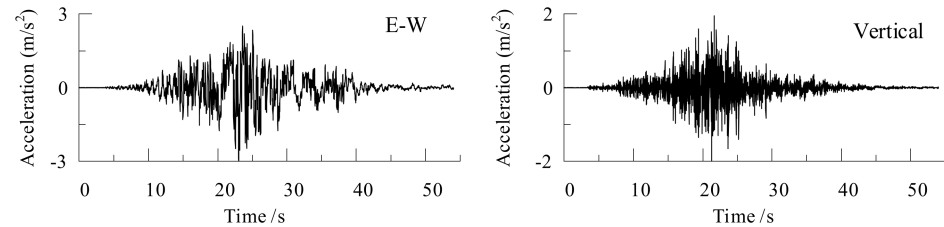


Figure 5. E–W and vertical components of the selected accelerogram A1.

The ovaling or racking deformation of the shotcrete, induced by the propagation of shear and pressure waves in the plane of the cross-section of the tunnel, is generally considered as the most critical deformation pattern during a seismic event. In this study, it can be inferred from Figure 6 that the horizontal component of motion generates shear deformations of the rock mass and then ovaling of the cavern cross-section, typical of that produced by a vertically propagating S wave. On the other hand, the application of the vertical component generates a deformation typical of a vertical propagating P wave.

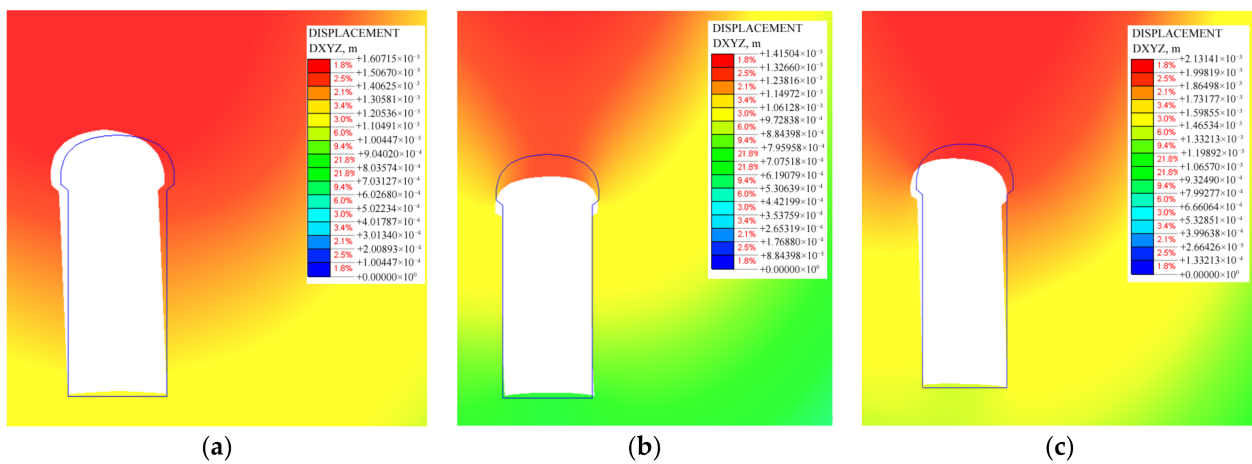


Figure 6. Deformed shapes of the cavern cross-section when the model is loaded by horizontal, i.e., E–W (a), vertical (b), and both components (c).

It is noted that the deformed shape and the displacements computed with the two components of motion can be derived by the superimposition of the results obtained for each component. This is due to the dynamic motion producing effects that are completely in the elastic field.

Figure 7 shows the distribution of the thrust force along the shotcrete lining when the horizontal, vertical, and both components are applied. The thrust induced by vertical motion is larger than that resulting from horizontal motion. Moreover, the thrust induced by both the components of motion is slightly smaller than the superimposition of the results of the two separate analyses. Moreover, the thrust force time history of the lateral bottom element, when subjected to three types of seismic input, is shown in Figure 8, and the results indicate that the thrust force of shotcrete is more dependent on P wave than on S wave in this case, which is in accordance with the conclusions obtained by Perino [27]. Accordingly, it may be concluded that the effect of P-wave propagation should be properly

considered during the seismic design of underground structures, though generally, only more attention has been given to the effect of shear wave propagation.

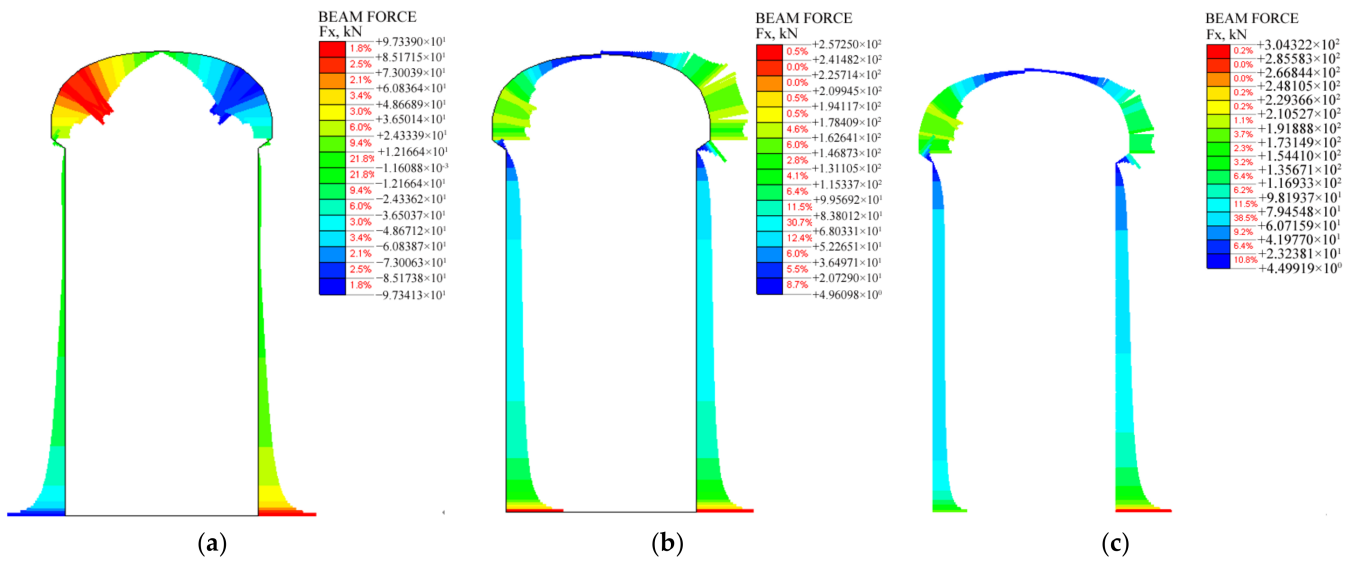


Figure 7. Thrust force along the shotcrete subjected to horizontal (a), vertical (b), and both (c) components of ground motion.

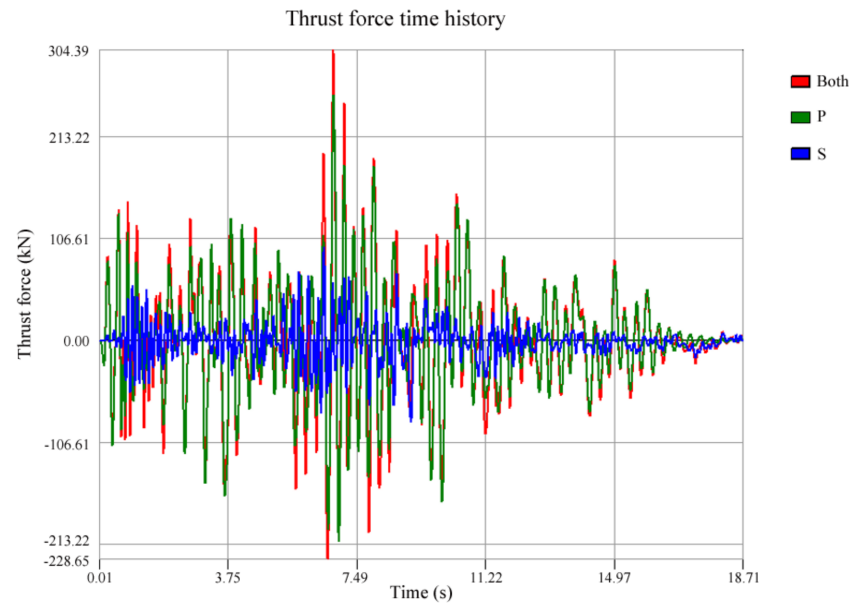
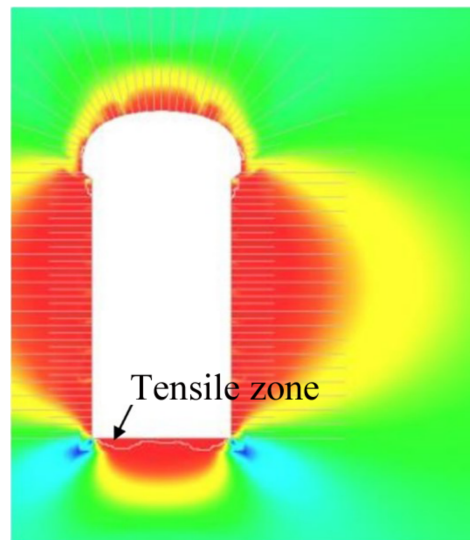


Figure 8. Thrust force time histories of the studied beam element subjected to P wave, S wave, and both waves.

Ground shaking by seismic events induces redistribution of stresses around the opening. Seven analyses using the selected seven groups of accelerograms containing two components (in the E–W and vertical directions) were performed, and the average seismic response could then be obtained. Figure 9 shows the average minimum principal stress distribution around the cavern induced after the application of the two components of motion. The maximum tensile stress value, equal to 0.5 MPa, is very close to the tensile strength (0.51 MPa).



**Figure 9.** Tensile zone distribution resulting from dynamic analyses.

5.2. 3D Analyses

Three-dimensional (3D) analyses of the entire cavern were performed with the seven groups of accelerograms in three directions being applied to the FEM model. The redistribution of stress around the cavern induced by additional seismic loading has been studied in Figure 10. The tensile zone around the cavern, when the dynamic effect is considered, is larger than that observed in the static case and consists of scattered tensile tiny failure zones at the opening contour. The minimum principal stress distribution along the longitudinal cross-section is shown in Figure 11, where the tensile zone is mainly concentrated at the sharp corners.

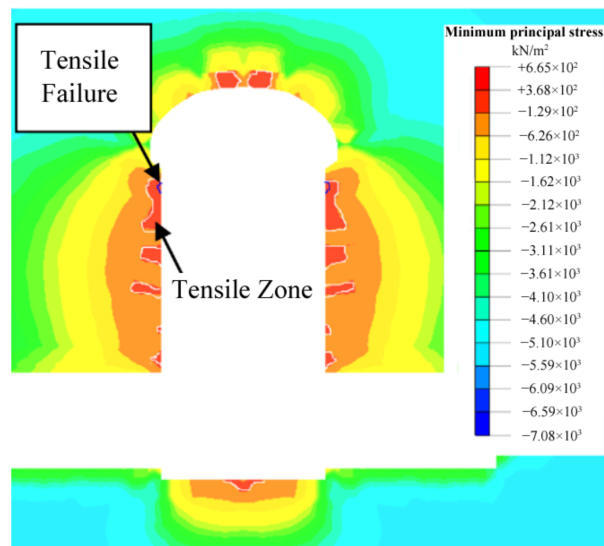


**Figure 10.** Minimum principal stress distribution after dynamic analysis.

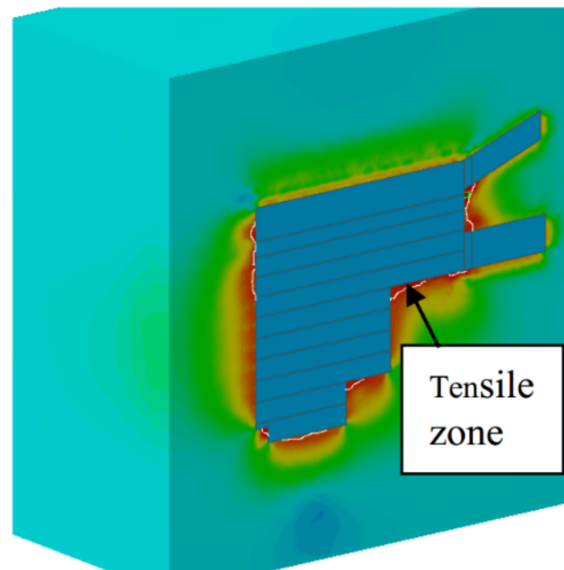


**Figure 11.** Tensile zone of longitudinal cross-section when considering dynamic effects.

Figure 12 shows the thrust in the shotcrete lining when the cavern undergoes the A1 seismic event. The values obtained are in good agreement with those derived from the 2D analysis shown in Figure 8. The 3D results for other seismic events are quite similar. Finally, the additional stresses in the short dowels and in the tensioned anchors induced by the seismic events are rather small.

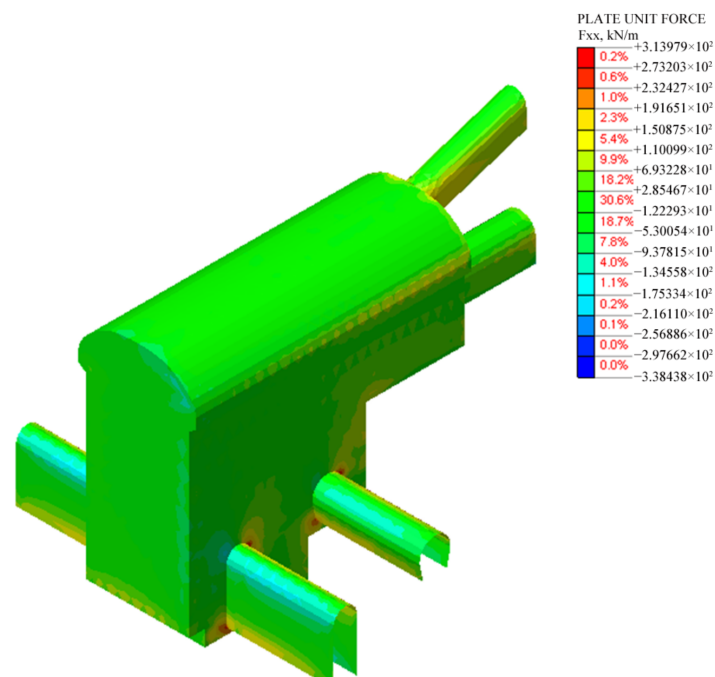


**Figure 12.** Thrust force of shotcrete induced by seismic loading.

## 6. Concluding Remarks

The comparison of the plastic-zone evolution and the distribution of principal stress surrounding the cavern in intrinsic and reinforced conditions indicates that the reinforcement system is very effective to control the development of the plastic zone, reduce the tensile stress, and hence further stabilize the rock mass. The systematic bolt reinforcement is an efficient earthquake countermeasure to significantly improve the seismic performance

and reduce the fragility of large-span underground structures (e.g., powerhouse cavern) under strong earthquake events.

The results obtained indicate that the 2D plane-strain model can serve as a complement to the 3D model, which gives reasonable predictions of the seismic response of the large-span powerhouse cavern. The proposed 2D model is expected to facilitate future detailed seismic response analysis of large underground caverns constructed in the past on the basis of seismic design analyses and input data from post-earthquake records recently made available, within the framework of modern performance-based design methodology.

**Author Contributions:** Conceptualization, Y.L. and L.W.; methodology, Y.L.; software, Y.C.; validation, L.W. and L.G.; formal analysis, Y.L.; investigation, Y.C. and S.L.; resources, L.W.; data curation, Y.L. and S.L.; writing—original draft preparation, Y.L.; writing—review and editing, L.W.; supervision, L.W.; project administration, L.W.; funding acquisition, L.W. All authors have read and agreed to the published version of the manuscript.

**Funding:** This research was funded by National Natural Science Fund, grant number 51978335, 51668002 and 52168044.

**Institutional Review Board Statement:** Not applicable.

**Informed Consent Statement:** Not applicable.

**Data Availability Statement:** Not applicable.

**Acknowledgments:** The authors are truly grateful for the financial support from the National Natural Science Fund (51978335, 51668002, 52168044), and also grateful to the High Performance Computing Center of Nanjing Tech University for supporting the computational resources.

**Conflicts of Interest:** The authors declare no conflict of interest.

## References

1. Hashash, Y.; Hook, J.; Schmidt, B.; Yao, J. Seismic design and analysis of underground structures. *Tunn. Undergr. Space Technol.* **2001**, *16*, 247–293. [[CrossRef](#)]
2. Wang, W.; Wang, T.; Su, J.; Lin, C.; Seng, C. Assessment of damages in mountain tunnels due to the Taiwan Chi-Chi earthquake. *Tunn. Undergr. Space Technol.* **2001**, *163*, 133–150. [[CrossRef](#)]
3. Lanzano, G.; Bilotta, E.; Russo, G. Tunnels under seismic loading: A review of damage case histories and Protection methods. In *Workshop of Mitigation of the Earthquake Effects in Towns and in Industrial Regional Districts*; University of Zagreb: Dubrovnik, Croatia, 2008; Volume 1971, pp. 1–10.
4. Liu, J.W.; Wang, Z.M.; Xie, F.R.; Li, Y.J. Seismic Hazard and risk Assessments in North China Based on the Historical Intensity Observations. *China Earthq. Eng. J.* **2014**, *36*, 134–143.
5. Zou, Y.; Jing, L.P.; Cui, J.; Li, Y.Q. Seismic Response Analysis of Box Tunnels in Saturated Sand. *China Earthq. Eng. J.* **2015**, *37*, 329–335.
6. Zhao, K.; Wang, Q.Z.; Chen, Q.; Zhuang, H.Y.; Chen, G.X. Simplified effective stress modeling of shear wave propagation in saturated granular soils. *Geotech. Lett.* **2021**, *11*, 1–9. [[CrossRef](#)]
7. Zhang, X.; Jiang, Y.J.; Sugimoto, S. Seismic damage assessment of mountain tunnel: A case study on the Tawarayama tunnel due to the 2016 Kumamoto Earthquake. *Tunn. Undergr. Space Technol.* **2018**, *71*, 138–148. [[CrossRef](#)]
8. Callisto, L.; Ricci, C. Interpretation and back-analysis of the damage observed in a deep tunnel after the 2016 Norcia earthquake in Italy. *Tunn. Undergr. Space Technol.* **2019**, *89*, 238–248. [[CrossRef](#)]
9. Dowding, C.H.; Rozen, A. Damage to rock tunnels from earthquake shaking. American Society of Civil Engineers. *ASCE J. Geotech. Eng. Div.* **1978**, *104*, 175–191. [[CrossRef](#)]
10. John, C.M.; Zahrah, T.F. Aseismic design of underground structures. *Tunn. Undergr. Space Technol.* **1987**, *2*, 165–197. [[CrossRef](#)]
11. Xiao, W.; Cheng, P. Review of seismic damage characteristics and influence factors of mountain tunnels. *Arab. J. Geosci.* **2022**, *15*, 478.
12. Yu, H.T.; Chen, G. Pseudo-static simplified analytical solution for seismic response of deep tunnels with arbitrary cross-section shapes. *Comput. Geotech.* **2021**, *137*, 104306. [[CrossRef](#)]
13. Yang, J.; Zhuang, H.Y.; Wang, W.; Zhou, Z.; Chen, G.X. Seismic performance and effective isolation of a large multilayered underground subway station. *Soil Dyn. Earthq. Eng.* **2021**, *141*, 106560.
14. Tiwari, R.; Lam, N. Displacement based seismic assessment of base restrained retaining walls. *Acta Geotech.* **2022**, 1–20. [[CrossRef](#)]
15. Zhuang, H.Y.; Yang, J.; Chen, S.; Dong, Z.; Chen, G.X. Statistical numerical method for determining seismic performance and fragility of shallow-buried underground structure. *Tunn. Undergr. Space Technol.* **2021**, *116*, 104090. [[CrossRef](#)]

16. Conte, E.; Pugliese, L.; Troncone, A. Earthquake-induced permanent displacements of embedded cantilever retaining walls. *Géotechnique* **2022**, *21*, 1–10. [[CrossRef](#)]
17. Miao, Y.; He, H.; Liu, H.; Wang, S. Reproducing ground response using in-situ soil dynamic parameters. *Earthq. Eng. Struct. Dyn.* **2022**, 1–17. [[CrossRef](#)]
18. Hoek, E.; Brown, E.T. Practical estimates of rock mass strength. *Int. J. Rock Mech. Min.* **1997**, *34*, 1165–1186. [[CrossRef](#)]
19. ISRM. ISRM suggested methods for rock stress estimation. *Int. J. Rock Mech. Min. Sci.* **2003**, *40*, 991–1025. [[CrossRef](#)]
20. Barla, G.; Fava, A.; Peri, G. Design and construction of the Venaus powerhouse cavern in calcschists. *Geomech. Tunn.* **2008**, *1*, 400–406. [[CrossRef](#)]
21. CEN. *Eurocode 8: Design of Structures for Earthquake Resistance: Part 1: General Rules, Seismic Actions and Rules for Buildings*; European Committee for Standardization: Brussels, Belgium, 2004.
22. Reiter, L. *Earthquake Hazard Analysis—Issues and Insights*; Columbia University Press: New York, NY, USA, 1990; Volume 254.
23. Midas-GTS. *Geotechnical and Tunnel Analysis System*; Midas Information Technology Co., Ltd.: Seongnam, Korea, 2010.
24. Day, R.A.; Potts, D.M. Zero thickness interface elements-numerical stability and application. *Int. J. Numer. Anal. Method Geomech.* **1994**, *18*, 689–708. [[CrossRef](#)]
25. Kuhlmeier, R.L.; Lysmer, J. Finite element method accuracy for wave propagation problems. *ASCE J. Soil Mech. Found. Div.* **1973**, *99*, 421–427. [[CrossRef](#)]
26. Zhao, K.; Wang, Q.Z.; Zhuang, H.Y.; Li, Z.Y.; Chen, G.X. A fully coupled flow deformation model for seismic site response analyses of liquefiable marine sediments. *Ocean Eng.* **2022**, *251*, 111144. [[CrossRef](#)]
27. Perino, A. *Wave Propagation through Discontinuous Media in Rock Engineering*. Ph.D. Thesis, Politecnico di Torino, Turin, Italy, May 2011.